IV International Conference on Particle-based Methods – Fundamentals and Applications
PARTICLES 2015
E. Oñate, M. Bischoff, D.R.J. Owen, P. Wriggers & T. Zohdi (Eds)

MODELLING THE FORMATION AND BREAKUP OF PARTICLE CLUSTERS IN METAL MELT SUBJECTED TO EXTERNAL FIELDS

ANTON MANOYLOV[1], VALDIS BOJAREVICS[1], KOULIS PERICLEOUS[1]

[1] Centre of Numerical Modelling and Process Analysis, University of Greenwich
30 Park Row, London, UK, SE10 9LS
A.Manoylov@gre.ac.uk, http://cnmpa.gre.ac.uk/group_cseg.html

Key words: Adhesion of particles, CFD-DEM, metal-matrix nano-composites

Abstract. Aluminium and magnesium based metal matrix nano-composites (MMNC) with ceramic nano-reinforcements promise low weight with high durability and superior strength, desirable properties in aerospace, automobile and other applications. However, due to the small size of the particles, adhesion force between becomes significant which leads to particle agglomeration. Large clusters of nano-particles are detrimental for the final properties of the MMNC. To prevent agglomeration and to break up clusters, ultrasonic processing is used via an immersed sonotrode, or alternatively via electromagnetic vibration. The collapse of the cavitation bubbles as a result of ultra-sonication is believed to be the main mechanism of breaking up the clusters of nano-particles. The complex interaction of flow and co-joint particles subjected to the shockwave induced by cavitation is addressed in detail using a discrete-element method (DEM) code. Adhesive, elastic and frictional forces between the particles are incorporated and various models of adhesion are compared.

1. INTRODUCTION

Metal matrix composites (MMC) form a class of advanced materials typically based on light metals such as Al and Mg and ceramic reinforcements including but not limited to Al2O3, AlN, SiC etc. Combining the light weight and ductility of Al and Mg with high strength and high modulus of ceramic materials makes MMC desirable for applications in aerospace and automotive industries. A good review of the development of MMCs is given in [1]. Metal matrix nano-composites (MMNC) is a recently developed subclass of MMCs based on nano-particle reinforcements.

MMNCs are manufactured by mixing the nano-particles into the metal melt. Recent papers showed a clear increase in the Young's modulus (by up to 100%) and in hardness (by up to 50%) of the matrix metal with the addition of carbon or ceramic nano-particles [[2]-[4]]. These studies however indicate that the nano-particles tend to form large clusters and that an even distribution of nanoparticles is needed to achieve the beneficial properties of MMNCs. The effect of the distribution of particles on the final properties of MMNCs is explained by the fact that large-size clusters no longer act as dislocation anchors, but instead become defects.

The agglomeration of particles in MMNCs is related to the fact that nano-sized inclusions have a larger ratio of surface area to the volume than e.g. micro-sized particles. This causes surface forces such as van der Waals interaction and adhesive contact to dominate over the volume forces such as e.g. inertia or elastic repulsion in the case of nano-particles.

Various mechanisms of detachment of adhered particles have been reported in the literature [5], which includes turbulent flow. It is expected that drag and shear forces in turbulent flow can improve separation of the particles and thus contribute to de-agglomeration. However, the drag force alone is not sufficient to de-agglomerate the nano-particles. This can be qualitatively illustrated by comparing the Stokes equation for the drag force with the force required to break two spherical particles apart, known as the pull off force, given by e.g. Bradley [5]:

$$6\pi\mu_f R u_f = 4\pi R_p \gamma_{sl} \quad (1)$$

where μ_f and u_f are the velocity and dynamic viscosity of the melt, and γ_{sl} is the solid-liquid interfacial energy. For the case of aluminium melt the dynamic viscosity is μ_f=0.0013 Pa•s. Assuming the interfacial energy γ_{sl} =0.2-2.0 J/m2, equation (1) yields u_f =100-1000 m/s. Such fluid velocity values can be locally achieved as a result of the collapse of cavitation bubbles induced by ultrasonic field. Indeed, applying an electro-magnetic stirring in combination with ultrasonic vibrations was found beneficial for nano-particle dispersion in metal melt [[2][5], [8]-[8]].

This paper concerns the investigation of forces causing the agglomeration of nano-particles and the conditions favouring breaking up of these agglomerations. A numerical model has been developed that simulates the response of the cluster of nano-particles to the shockwave induced by the collapse of cavitation bubbles. The collisions of the particles are treated individually using the DEM approach, as opposed to the population balance methods where collisions are using the kinetic theory of granular flow as in e.g. [8]. It is proposed to investigate the behaviour of NPs in metal melts subjected to electro-magnetic [8] and other external fields using a coupled CFD-DEM model similar to that developed by Goniva et al [9] and Hager et al [11]. Whilst a fully coupled CFD-DEM solver is under development, this paper presents results obtained at the scale of a single nano-particle. Authors of this paper reported the results earlier [12], however some theoretical aspects of the modelling are explained in more details in this paper.

2. REVIEW OF ADHESION THEORIES

Bradley [5] first described the van der Waals force acting between two rigid spheres in contact and calculated the pull off force as $P_c=4\pi\gamma R$, where γ is interfacial energy of the contacting materials [1] and R is the radius of the sphere.

Derjaguin [13] pointed out that elastic deformations of the spheres need to be accounted for as well as the adhesive interactions. He presented the first attempt to consider the problem of adhesion between elastic spheres: calculating the deformations of the spheres using Hertzian contact theory, he evaluated the work of adhesion assuming only the pair-wise interactions of the closest surface elements. The interaction energy between small elements of curved surfaces was assumed the same as for parallel planes which is known as the Derjaguin approximation.

On the other hand, Johnson [14] made an attempt to solve the adhesive contact problem by combining the Hertzian spherical contact problem and the problem of a rigid flat-ended punch. Johnson et al. [15] applied Derjaguin's idea to equate the work done by the surface attractions against the work of deformation in the elastic spheres to Johnson's [14] combined stress superposition. This resulted in the creation of the famous **JKR** (Johnson, Kendall, and Roberts)

[1] The formulae for the pull off force of adhered particles are often used with the notation $\Delta\gamma$ which is the *work of adhesion*. For spheres of the same material $\Delta\gamma \approx \gamma/2$, therefore $P_c=2\pi\Delta\gamma R$

theory of adhesive contact. According to them the attractive adhesion force is acting only over the contact area and significantly affects the shapes of the contacting spherical bodies. The pull off force calculated using JKR model is $P_c=3\pi\gamma R$. The contact area is a circle with radius a, defined as follows:

$$a^3 = \frac{3R}{4E}\left[P + 6\pi\gamma R + \sqrt{12P\pi\gamma R + 36\pi^2\gamma^2R^2}\right], \quad (2)$$

where P is the applied normal load and E is the combined Young's modulus. Hertzian theory evaluates the contact radius simply as $a^3=3PR/4E$, therefore JKR theory is reduced to Hertzian if adhesion is neglected, i.e γ=0.

Derjaguin et al [16] developed a contact theory (**DMT –** Derjaguin, Müller, Toporov) that combined Bradley's adhesion force with Hertz elastic contact theory. The attractive intermolecular force is assumed applicable in the contact area as well as in the surrounding annulus zone. The resulting profile of the deformed spheres remains Hertzian and the pull off force is equal to the one derived by Bradley, $P_c=4\pi\gamma R$. The contact radius is then given by

$$a^3 = \frac{3R}{4E}[P + 4\pi\gamma R] \quad (3)$$

Qualitative analysis of both JKR and DMT models performed by Tabor [17] as well as more detailed analysis based on the Lennard-Jones potential conducted by Muller et al [18] showed that the contradiction between the models lies in the physical principles of adhesive contact assumed by the authors. Both Tabor and Muller concluded that the adhesive contact of larger, softer bodies with stronger surface interaction can be described by the JKR model, while the DMT model is applicable to the smaller, harder bodies with weaker surface interaction. Parameters τ, μ were introduced in [17] and [18] to determine which model is more appropriate:

$$\tau \cong \left[\frac{R\gamma^2}{E^2 z_0^3}\right]^{1/3}, \ \mu = \frac{32}{3\pi}\left[\frac{2R\gamma^2}{\pi E^2 z_0^3}\right]^{1/3}, \quad (4)$$

where z_0 is the equilibrium separation distance, typically 0.16-0.4 nm [19]. According to Muller if μ<1 then DMT is applicable whereas if μ>>1 it is JKR.

Maugis [20] suggested a smooth transition model between JKR and DMT approaches which exploits the principles of fracture mechanics. For simplicity, Lennard-Jones interaction potential is replaced by the step-function, which is known as Dugdale approximation. Greenwood and Johnson [21] suggested an alternative model to Maugis based on a combination of two Hertzian profiles that also connect both the JKR and DMT models in one general theory. These two models use a parameter, which defines the area where the adhesion force is applicable. The necessity to evaluate this parameter at every time step during particle collision makes it impractical to use either Maugis [20] or Greenwood and Johnson [21] theories in a DEM solver. Therefore in the present paper the JKR and DMT models are implemented and the Müller parameter μ is used to determine which one is more applicable.

3. CONTACT MECHANICS

3.1. Oblique loading without adhesion.

The most commonly used particle contact model was first introduced by Cundall and Strack [22] in attempt to predict the complex behaviour of sand specimens under loading and unloading. They suggested treating sand particles as spheres which can move individually and

interact only at the contact spots. The contact model consisted of linear spring elements as well and viscous damping elements in both normal and tangential directions, as shown schematically in Figure 1a. The modifications of this model are reviewed in e.g. [23] [24]. The developments of this approach can include addition of rolling and twisting resistance [25] which are neglected in this paper.

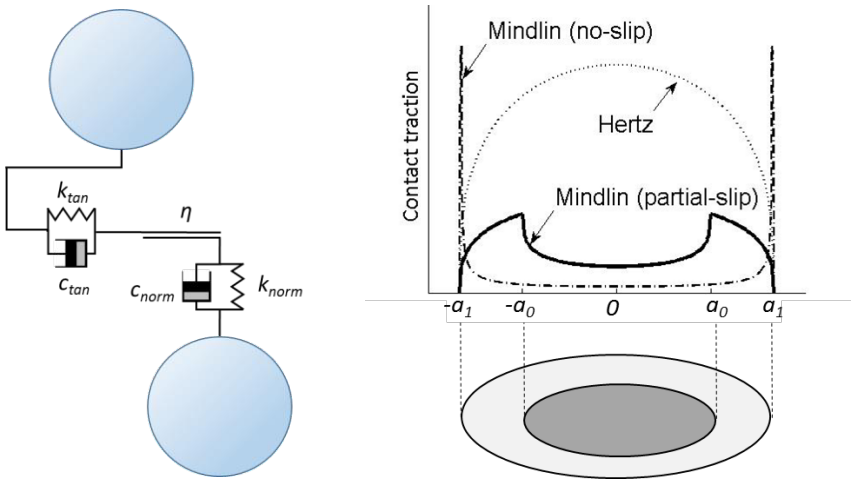

Figure 1 (a) Commonly used spring-dashpot and sliding element model; **(b)** contact traction distribution of two contacting spherical bodies according to the Mindlin and Deresiewicz model. ▭ - indicates circular zone with radius a_0 where elastic tangential force is applicable, ▭ - indicates the ring-shaped micro-slip area with external radius a_1..

While being extensively used in CFD-DEM simulation codes such as developed by Goniva, Kloss, Hager, Wierink and colleagues [9], [11], this model has a number of disadvantages. Firstly, accurate description of the contact between spherical bodies given by Hertz predicts non-linear normal elastic stiffness as $k_n=2E^*a$, where E^* is the combined Young's modulus and a is the radius of the (circular) contact area. It is noted in [25] that for small deformations Cundall and Strack model works well, although it is not obvious how to correlate the constant elastic stiffness values k_{norm}, k_{tan} and viscous damping coefficients c_{norm}, c_{tan} with properties of the materials involved. In addition to that, this paper considers nano-particles of sizes 50 nm to 1 μm, and therefore adhesion force must be incorporated. All of the adhesion models mentioned in the Section 2 of this paper are based on Hertz elastic theory. For these reasons, Hertz theory is used in this paper to evaluate the relationships between normal force and displacement as well as contact area.

The tangential contact forces are implemented in this paper by means of the Mindlin and Deresiewicz theory [26]. It is assumed that two elastic spheres in tangential contact experience a partial-slip, where the total force is a combination of elastic tangential force in the circular area in the centre of the contact zone and sliding friction force in the ring shaped exterior of the contact zone. Once the partial-slip tangential force exceeds the total sliding friction force, the bodies slide relative to each other. The tangential force in this case is then equivalent to the sliding friction force $F_s=\eta P$, where η is the friction coefficient, P is the normal load. The distribution of contact traction is illustrated in Figure 1b.

Thornton and Yin [27] combined all the major cases of the loading/unloading conditions described by Mindlin & Deresievicz [26] and derived the following expression for the tangential stiffness during oblique loading:

$$k^t = 8G^* a\theta \pm \eta(1-\theta)\frac{\Delta P}{\Delta \delta_t} \tag{5}$$

where G^* is the combined shear modulus, a is the contact radius, η is the friction coefficient, ΔP is the increment of the normal load, $\Delta\delta_t$ is the increment of the tangential displacement and θ is a parameter defining the ratio of the elastic force to the micro slip friction force. The parameter θ depends on the loading history and is defined as follows:

$$\underset{\text{for loading}}{\theta^3 = 1 - \frac{T+\eta\Delta P}{\eta P}}; \qquad \underset{\text{for unloading}}{\theta^3 = 1 - \frac{T^* - T + 2\eta\Delta P}{2\eta P}}; \qquad \underset{\text{for reloading}}{\theta^3 = 1 - \frac{T - T^{**} + 2\eta\Delta P}{2\eta P}}, \tag{6}$$

where T is current value of the tangential force and T^* and T^{**} are the load reversal points. Normal elastic stiffness is defined as $k^n=2E^*a$ according to Hertz theory; see [27] for details.

3.2. Oblique contact with JKR adhesion

Savkoor and Briggs [28] extended the JKR contact theory to consider the effect of adhesion in the case of oblique loading. It was suggested that applying the tangential force reduces the potential energy by an amount of $T\delta_t/2$. Adding this term to the JKR energy balance equation modified the contact radius (1) as:

$$a^3 = \frac{3R}{4E}\left[P + 6\pi\gamma R \pm \sqrt{12P\pi\gamma R + 36\pi^2\gamma^2R^2 - \frac{T^2E}{4G}}\right] \tag{7}$$

It was concluded that in the presence of tangential force, the contacting spheres peel off each other thus reducing the contact area. The peeling process continues until T reaches the critical value of

$$T_c = 4\sqrt{(3P\pi\gamma R + 9\pi^2\gamma^2R^2)\mathrm{G/E}}. \tag{8}$$

For the normal load Thornton and Yin [21] have adopted the JKT theory. The stiffness is then evaluated as

$$k^n = 2E^* a\left[3 - 3\left(\frac{a_c}{a}\right)^{\frac{3}{2}}\right] / \left[3 - \left(\frac{a_c}{a}\right)^{\frac{3}{2}}\right] \tag{9}$$

where $a_c=9\pi\gamma R^2/4E$ is the JKR contact radius at the moment of separation (pull off radius).

In the case of oblique loading Thornton and Yin [27] followed [28] in what concerns the peeling process. They however assumed that once the peeling process is complete, the contacting bodies operate in the partial slip regime as described before with the difference that the normal force P is replaced with $P+6\pi\gamma R$.

3.3. Oblique contact with DMT adhesion.

In this paper it is suggested to combine the Thornton and Yin [27] partial slip no adhesion model with DMT adhesion. The DMT theory assumes that the deformed shapes of the contacting bodies remain within Hertzian elastic theory. Therefore a no-adhesion model [27]

was adopted where the normal force P is replaced with $P+4\pi\gamma R$ to account for the adhesion force. This approach considers instantaneous separation of the particles, as opposed to the JKR theory, where particles stretch elastically prior to pulling off. The maximum stretching in the JKR case is evaluated as $\delta_c = \left(\frac{3\pi^2\gamma^2 R}{16E^2}\right)^{1/3}$ whereas δ_c=0 in the DMT case. The effect of the stretching prior to separation is illustrated in the results section.

4. VISCOUS DRAG

The momentum of the fluid is transferred on the particles via the drag force. Di Felice's [29] theory is used to account for the effect of presence of other particles. Drag force on a single particle in a flow with relative velocity $v = v_f - v_p$, where v_f, v_p are the velocities of the fluid and the particle, can be evaluated as follows:

$$\begin{aligned} F_d &= \tfrac{1}{2}\rho_f v^2 \mathrm{C}_d \pi R_p^2 \varepsilon^{-\beta} \\ \mathrm{C_d} &= \left(0.63 + \frac{4.8}{\sqrt{\mathrm{Re_p}}}\right)^2 \\ Re_p &= \frac{\rho_f}{\mu_f}\alpha_f R_p |v_f - v_p| \end{aligned} \tag{10}$$

where Re_p is the particle Reynolds number, μ_f and ρ_f are dynamic viscosity and density of the fluid, ε is the void fraction value, C_d is the drag coefficient for spherical particles, and function $g(\varepsilon) = \varepsilon^{-\beta}$ is a measure of how much the drag force is affected by the presence of other particles. Empirical parameter β was evaluated to fit the experimental data for a wide range of Reynolds numbers (10^{-2} to 10^4) and void fraction values (0.4 to 1):

$$\beta = 3.7 - 0.65e^{-0.5\left(1.5 - log_{10} Re_p\right)^2} \tag{11}$$

In the literature, modifications of $g(\varepsilon)$ are used, such as $g(\varepsilon) = \varepsilon^{1-\beta}$ [24], $g(\varepsilon) = \varepsilon^{2-\beta}$ [9][11], [23], or $g(\varepsilon) = \varepsilon^{-1-\beta}$ [30]. Di Felice noted however that in the case of the flow through random packed spheres (ε≈0.4), Ergun's equation predicts $g(0.4) = \frac{14.6}{C_d}\left(1 + \frac{51.4}{Re_p}\right)$. For a wide range of Reynolds numbers $g(0.4)$ is best predicted by $g(\varepsilon) = \varepsilon^{-\beta}$. In e.g. [25] Stokes drag formula is used multiplied by $g(\varepsilon) = \varepsilon^{-\beta}$.

The void fraction value ε is typically evaluated based on the density of particles in a mesh cell (see e.g. [9], [9][11]). In the present model the CFD mesh is not defined, therefore the void fraction is evaluated based on the cubic cell $10R_p \times 10R_p \times 10R_p$ centred at the particle centre.

5. MODELLING THE BREAKING UP OF NANO-PARTICLE AGGLOMERATES

Two-dimensional densely packed agglomerates of 36 and 37 mono-sized spherical particles were considered as shown in Figure 2. For simplicity, all the forces were assumed acting in the X and Z direction only, and the problem was modelled in two dimensions. Mass, volume, void fraction and contact area were however evaluated assuming that particles are spherical rather than circular. Both normal and tangential contact forces were modelled based on [27] and both JKR and DMT models of adhesion were adopted. The particle material properties are those of SiC and fluid properties are those of liquid aluminium. These and other parameters used in the simulations are provided in Table 1.

Table 1 Particle and fluid properties used in the simulations

Property		Value(s)	Units
Radius	R	50 to 1000	nm
Young's modulus	E	450	GPa
Poison's raito	ν	0.185	-
Particle density	ρ_p	3160	kg/m^3
Friction coefficient	η	0.3	-
Fluid density	ρ_f	2375	kg/m^3
Dynamic viscosity	μ_f	0.0013	Pa·S
Interfacial energy	γ	0.02 to 2.0	J/m^2

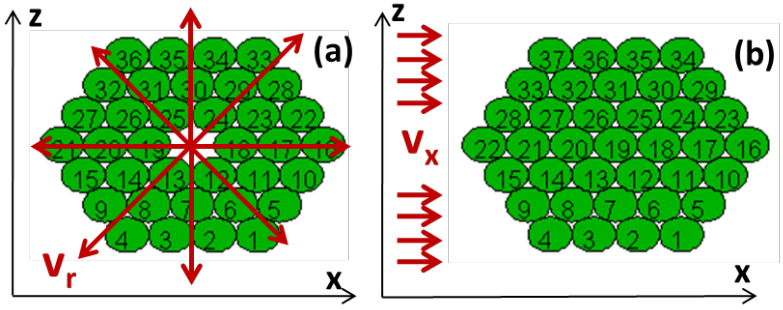

Figure 2 (a) Cluster of 36 particles subjected to the spherical velocity pulse V_r originating in the centre of the cluster. (b) Cluster of 37 particles subjected to lateral velocity pulse V_x.

5.1. Collapsing of Gas Bubbles.

It is known from various sources that ultrasound has a beneficial effect on de-agglomeration of the nano-particle clusters [[2][5], [8]-[8]]. This is explained by the phenomenon of acoustic cavitation, which includes the formation, growth, pulsation and collapse of gas bubbles. These processes are accompanied by the creation of "hotspots" – zones of high temperature and pressure which explain the beneficial effect of ultrasonic vibrations on breaking the clusters and the dispersing of nano-particles [4]. As a result of the implosive collapse of the bubbles high amplitude shockwaves are generated. In [7] authors compare the pressure peak occurring as a result of the collapse with the pressure required to separate two individual nano-particles held together by van der Waals and capillary forces. It is however expected that due to complex pair-wise contact interactions between the particles in a cluster, it is more difficult to de-agglomerate a cluster of particles rather than two individual particles. For this reason the behaviour of a cluster of nano-particles subjected to the shockwave is investigated in this paper.

5.2. Lateral And Spherical Pulses.

In this paper a possibility is also investigated that the agglomerates of nano-particles contain gas bubbles inside (typically hydrogen), originating due to poor wettability of the nano-particles and the specifics of the manufacturing process. In the case of collapsing of a bubble inside of the agglomerate a spherical shockwave is considered radiating from the centre of the cluster as shown in Figure 2a. In [12] authors have also considered lateral pulse originating on the side of the cluster Figure 2b. It was however shown, that lateral pulse causes the cluster to move as a whole, which makes it more difficult to study the de-agglomeration mechanisms.

The behaviour of the gas bubbles in the presence of the ultrasonic waves is a complex problem depending on multiple parameters, and is not studied in this paper. For simplicity it is assumed that the shockwave generated by the collapse of a gas bubble can be described as a rapidly decaying disturbance of the local velocity with an exponential time dependency. Expressing the shockwave as a velocity pulse allows the concentration of the particles to be taken into account using di Felice's approach (equation (10)). The details of the behaviour of the gaseous-fluid interface during the bubble collapse are not studied in this paper; therefore the duration τ of the pulse is covering a wide range from 5 ns to 5 μs in order to investigate a potential effect of the pulse duration. The magnitude of the pulse is defined by the maximum value v_0 which in this paper is ranging from 1-1000 m/s. In [7] authors estimated the cavitation pressure peak as $6 \cdot 10^7$ Pa if a bubble of initial size 100 μm collapses, and $1.5 \cdot 10^{10}$ if initial size is 1 μm. Using Bernoulli's equation, these peak pressure values can be correlated with the peak velocities of 225 m/s and 3575 m/s respectively.

$$F_d = \frac{1}{2}\rho_f v^2 \mathrm{C}_d \pi R_p^2 \varepsilon^{-\beta}$$

$$\mathrm{C_d} = \left(0.63 + \frac{4.8}{\sqrt{\mathrm{Re_p}}}\right)^2$$

$$Re_p = \frac{\rho_f}{\mu_f}\alpha_f R_p |v_f - v_p|$$

5.3. Interfacial Energy.

The interfacial energy γ of the contacting particles can be evaluated from the van der Waals attraction force acting between two flat surfaces separated by an equilibrium distance z_0 :

$$\gamma = \frac{A}{24\pi z_0^2} \tag{12}$$

where *A* is the Hamaker constant of the material. If particles are interacting in a medium, then Hamaker constant must be modified according to the rule:

$$A_{121} = \left(\sqrt{A_1} - \sqrt{A_2}\right)^2 \tag{13}$$

where A_1 and A_2 are the properties of the particles and the medium respectively [19]. The average separation distance z_0 for contacting solids with close packed atomic structure can be evaluated as σ/2.5, where σ is the interatomic distance. The typical value of σ=4 Å yields z_0=0.165 nm (see [19], page 277). Equations (12, 13) can be used to compute the interfacial energy for most solids and liquids. This theory is however not applicable to the system that involves liquid metals or other highly conducting fluids due to short-range non-additive electron exchange interaction. For this reason, a series of the interfacial energy values 0.02, 0.2 and 2.0 J/m^2 to cover a wide range of interfacial energies. In another paper by authors [12] the interfacial energy values 2.1 J/m^2 and 2.6 J/m^2 corresponding to aluminium oxide and silicon carbide particles in aluminium melt are used.

6. RESULTS AND DISCUSSION

6.1. The Effect Of The Contact Model.

In this section the effect of the adhesion model on breaking up of the nano-particles cluster via the spherical shockwave is investigated. Figure 3 shows the positions of the particles after

the incidence of the velocity pulse. The pulse duration is 50 ns, amplitudes 1 to 50 m/s, particles radius is 50 nm and interfacial energy γ_{sl}=0.2 J/m^2. Here and henceforth the particles belonging to the same sub-cluster are coloured and numbered for convenience. Individual particles are coloured red and have unique numbers. As expected, the no adhesion model (3rd row in Figure 3) predicts that all of the particles become isolated, since particles interact only via friction and elastic forces. As for adhesion models, it can be visually observed that particles tend to form chains of particles in the JKR case (2nd row in Figure 3) and more compact sub-clusters when the DMT model is used (1st row in Figure 3). This can be explained by, firstly, a lower pull off force of the JKR model and, secondly, by the JKR assumption that bodies do not separate instantaneously, but stretch while maintaining contact until the stretching becomes critical and pull off force is reached. This stretching extends the duration of the contact between the particles thus allowing them to re-agglomerate due to collisions with other particles. The analysis of the adhesion models clearly demonstrates that choice of the model may significantly affect the prediction of de-agglomeration.

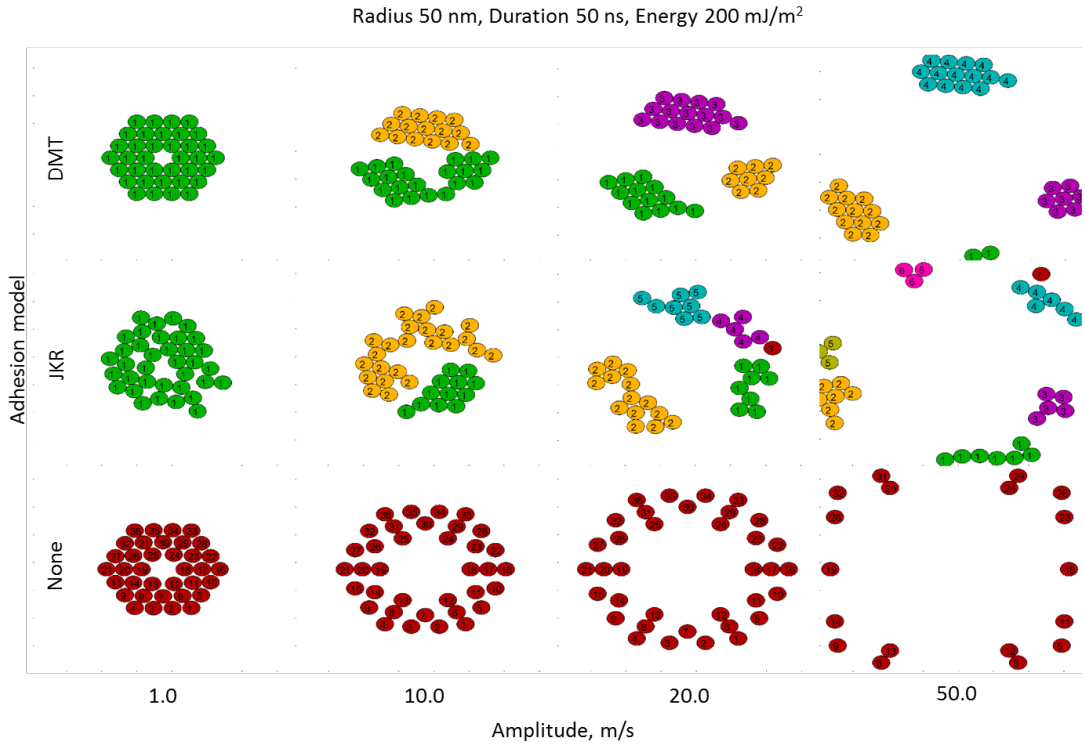

Figure 3 The effect of the adhesion model on breaking up of nano-particle clusters via spherical shockwave.

6.2. The Effect Of The Interfacial Energy.

In this section the results are shown for particles of radius 500 nm with interfacial energy values 0, 0.02, 0.2 and 2.0 J/m^2. The pulse duration is 500 ns and amplitudes 1.0 to 50.0 m/s. It can be observed from e.g. 3rd row in Figure 4 that particles with higher interfacial energy tend

to form large sub clusters during de-agglomeration. Particles with lower interfacial energy (see e.g. 2nd row in Figure 4) form smaller sub-clusters or individual particles. Same effect has been reported by authors [12] and terms "local" and "global" de-agglomeration were introduced. It was noticed that although global de-agglomeration may separate pieces further apart, the locally de-agglomerated particles can be dispersed by turbulent fluctuations or Brownian motion. For this reason global and local de-agglomeration should be evaluated separately.

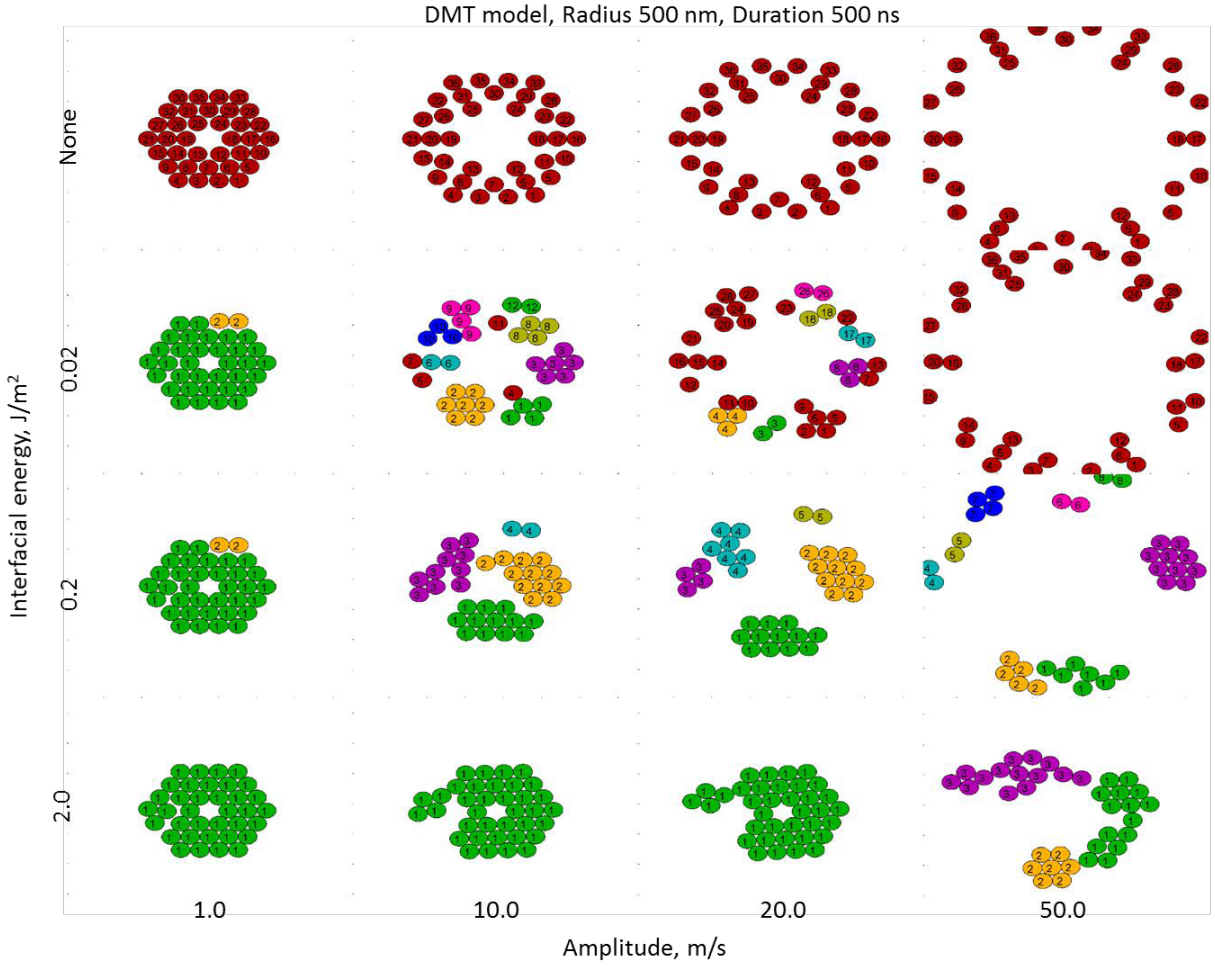

Figure 4 The effect of the interfacial energy on breaking up of nano-particle clusters via spherical shockwave.

7. CONCLUSIONS

A DEM model was developed in order to study the behaviour of a cluster of nano-particles subjected to the shockwave originating in the centre of the cluster. The model incorporates Mindlin and Deresiewicz partial-slip tangential contact theory and both JKR and DMT adhesion force theories. Drag force is implemented using di Felice approach based on the local concentration of particles. The effect of the adhesion model choice was studied and it was shown that JKR model predicts catenulate, chain-like structures whereas in the case of DMT model compact sub-clusters are formed. The behaviour of particles with various interfacial energies was compared, and it was found, that de-agglomerating particles with lower energies

result in smaller sub-clusters and more isolated particles, while under similar conditions particles with higher energies form larger sub-clusters. It is suggested that the effectiveness of the local and global de-agglomeration must be evaluated separately.

This study of the particle-particle interaction forces under various conditions is a part of an ongoing investigation of the mechanisms of de-agglomeration and is expected to help optimizing the electro-magnetic stirring and the ultrasonic processing of the metal melt with added nano-particles.

8. ACKNOWLEDGMENTS

The authors acknowledge financial support from the ExoMet Project (co-funded by the European Commission (contract FP7-NMP3-LA-2012-280421), by the European Space Agency and by the individual partner organizations).

9. REFERENCES

[1]. Ibrahim, I.A., Mohamed, F. A. and Lavernia, E. J. Particulate reinforced metal matrix composites – a review, *Journal of Material Science* (1991) 26:1137-1156.

[2]. Vorozhtsov S. et al. Physico-mechanical and electrical properties of aluminium-based composite materials with carbon nanoparticles *Light Metals* (2014), TMS, John Grandfield (Ed.), TMS, Warrendale, PA, 2014

[3]. Tamayo-Ariztondo, J. et al. Nanoparticles distribution and mechanical properties of aluminium MMNC treated with external fields. *Light Metals* (2014), TMS, John Grandfield (Ed.), TMS, Warrendale, PA, 2014

[4]. Yang, Y., Lan, J. and Li, X. Study on bulk aluminium MMNC fabricated by ultrasonic dispersion of nano-sized SiC particles in molten aluminium alloy. *Materials Science and Engineering A*, (2004) 380:378–383.

[5]. Soltani, M. and Ahmadi, G. On particle adhesion and removal mechanisms in turbulent flow. *Journal of Adhesion Science and Technology* (1994) 8(7):763-785.

[6]. Bradley, R. S. The Cohesive force between Solid Surfaces and the Surface Energy of solids *Phil. Mag.* (1932) 13:853–62,

[7]. Li, X., Yang, Y., Weiss, D. Ultrasonic cavitation based dispersion of nanoparticles in aluminium melts for solidification processing of bulk aluminium matrix nano-composite: Theoretical study, fabrication and characterization", *AFS Transactions, American Foundry Society*, Schaumburg, IL, USA (2007)

[8]. Zhang, D., Nastac, L. , Numerical modelling of the dispersion of ceramic nanoparticles during ultrasonic processing of aluminium-based nano-composites. *Journal of Materials Research and Technology* (2014) 3(4):296-302

[9]. Djambazov, G. et al. Contactless Acoustic Wave Generation in a Melt by Electromagnetic Induction *Light Metals* (2014), TMS, John Grandfield (Ed.), TMS, Warrendale, PA, 2014

[10]. Goniva C., et al., "A MULTI-PURPOSE OPEN SOURCE CFD-DEM APPROACH" 8th International Conference on CFD in Oil & Gas, Metallurgical and Process Industries, SINTEF/NTNU, Trondheim Norway, 21-23 June 2011

[11]. Hager, A et al. Parallel Resolved Open Source CFD-DEM: Method, Validation and Application. *The Journal of Computational Multiphase Flows*, (2014) 6(1):13-27.

[12]. Manoylov, A., Bojarevics, V., Pericleous, K. A. Modeling the Break-up of Nano-

particle Clusters in Aluminium- and Magnesium-Based Metal Matrix Nano-Composites. *Metallurgical and Materials Transactions. A* (2015) 46(7): 2893-2907
[13]. Derjaguin, B. Untersuchungen über die Reibung und Adhäsion, IV. 1. Theorie des Anhaftens kleiner Teilchen. *Kolloid-Zeitschrift* (1934) 69:155-164.
[14]. Johnson, K. L. A note on the adhesion of elastic solids. *British Journal of Applied Physics* (1958) 9:199-200.
[15]. Johnson, K.L., Kendall, K. and Roberts, A.D. Surface Energy and the Contact of Elastic Solids. *Proceedings of the Royal Society A.* (1971)324:301–13
[16]. Derjaguin, B.V., Muller, V.M. and Toporov, Y.P. Effect of Contact Deformations on the Adhesion of Particles. *Journal Colloid and Interface Science* (1975):53(2)
[17]. Tabor, D. Surface Forces and Surface Interactions. *Journal Colloid and Interface Science* (1977) 58(1)
[18]. Muller, V.M., Yushenko V. S. and Derjaguin, B.V. On the Influence of Molecular Forces on the Deformation of an Elastic Sphere and Its Sticking to a Rigid Plane. *Journal Colloid and Interface Science*. (1980) 77(1)
[19]. Israelachvili, J. N., *Intermolecular and Surface Forces*, Academic Press, New York, (1985).
[20]. Maugis, D. Adhesion of Spheres: The JKR-DMT Transition Using a Dugdale Model. *Journal Colloid and Interface Science.* (1992) 150(1)
[21]. Greenwood, J. A., Johnson, K. L. An alternative to the Maugis model of adhesion between elastic spheres. *J. Phys. D: Appl. Phys*. (1998) 31:3279–3290
[22]. Cundall, P. A., Strack, O. D. L. A discrete numerical model for granular assemblies. *Geotechique* (1979) 20(1): 47-65.
[23]. Zhou, Z. Y., Kuang, S. B., Chu, K. W., Yu, A. B. Discrete particle simulation of particle–fluid flow: model formulations and their applicability. *J. Fluid Mech.* (2010) 661: 482–510.
[24]. Zhu, H.P., Zhou, Z.Y., Yang, R.Y., Yu, A.B. Discrete particle simulation of particulate systems: Theoretical developments. *Chemical Engineering Science* (2007) 62:3378 – 3396
[25]. Marshall, J. S., Discrete-element modelling of particulate aerosol flows. *J. Comp. Physics* (2009) 228:1541-1561
[26]. Mindlin R. D. and Deresiewicz H. Elastic Spheres in Contact Under Varying Oblique forces. *J. Appl. Mech., Trans. ASME* (1953) 20:327.
[27]. Thornton, C., Yin, K. K. Impact of elastic spheres with and without adhesion. *Powder Technology* (1991) 65:153-166
[28]. Savkoor A.R. and Briggs, G. A. D. The Effect of Tangential Force on the Contact of Elastic Solids in Adhesion. *Proc. Roy. Soc. A* (1977) 356:103
[29]. Di Felice, R. The voidage function for fluid-particle interaction systems. *Int. J. Multiphase Flow*(1994) 20(I):153-159
[30]. Kafui, K.D., Thornton, C., Adams, M. J. Discrete particle-continuum fluid modelling of gas-solid fluidised beds. *Chem. Eng. Science* (2002) 57:2395-2410